

# Predicting graphene's nonlinear-optical refractive response for propagating pulses

David Castelló-Lurbe,<sup>1,\*</sup> Hugo Thienpont,<sup>1</sup> and Nathalie Vermeulen<sup>1</sup>

<sup>1</sup>*Brussels Photonics, Department of Applied Physics and Photonics, Vrije Universiteit Brussel, Pleinlaan 2, 1050 Brussel, Belgium*

(Dated: June 1, 2022)

## Abstract

The nonlinear-optical refractive behavior of a wide range of materials is typically described by means of perturbation theory near equilibrium. Graphene, however, can easily move far away from its equilibrium state after optical pumping, yielding strong nonlinear responses that cannot be modeled as mere perturbations. So far, it has been challenging to make theoretical predictions for these strong effects and to account for their evolution in time and space. Here, we present population-recipe-based expressions for graphene's nonlinear coefficients which immediately allow calculating the time- and propagation-length-dependent nonlinear effects outside the perturbative regime. Our framework successfully predicts both the nonlinearity magnitudes and signs observed in different experiments with graphene while also being compatible with the nonlinear pulse propagation formalism commonly used for waveguides.

---

\* dcastell@b-phot.org

## I. INTRODUCTION

Over the past decade there has been a rapidly growing interest in the theoretical [1, 2] and experimental [3–13] investigation of nonlinear-optical refraction in graphene using free-space and waveguided excitation configurations. This new research field was pioneered by the experiments of Hendry *et al.* showing an exceptionally large effective graphene nonlinearity  $|\chi_{\text{gr}}^{(3)}| \sim 10^{-7} \text{ esu} \sim 10^5 \chi_{\text{Si}}^{(3)}$  [3] or, equivalently, an effective nonlinear index  $|n_{2,\text{gr}}| \sim 10^{-13} \text{ m}^2 \text{ W}^{-1}$ . The research results reported since then seem to point in different directions, and have made it a major challenge to fully understand graphenes nonlinear-optical behavior. Indeed, the experimental data include both positive- [4, 9] and negative-valued [6–8, 13] effective nonlinearities with a magnitude compatible with that of Hendry's experiments [3], as well as much smaller nonlinearities [10]. From a theoretical point-of-view, calculations for the perturbative nonlinearity  $\chi_{\text{gr}}^{(3)}$  [1, 2] give rise to nonlinearities that are two orders of magnitude smaller than  $|\chi_{\text{gr}}^{(3)}| \sim 10^{-7} \text{ esu}$  measured in the aforementioned experiments. Strictly speaking, using perturbation theory implies that the graphene sheet remains close to its initial equilibrium state, but this is not necessarily the case in practice [14].

Most of the experiments carried out so far were conducted using an exfoliated or chemical-vapor-deposition(CVD)-grown graphene sample without intentional doping. As such, when using optical excitation wavelengths, one-photon absorption (1PA) in the graphene layer is unavoidable, and the resulting free-carrier generation can give rise to nonlinearities *outside* the perturbative regime with strong changes not only in temperature [11] but also in chemical potential [12]. What is more, our recent investigations on self-phase modulation in graphene-covered waveguides have shown that these non-perturbative graphene nonlinearities can dominate over their perturbative counterparts, with saturation playing an important role in the carrier dynamics. For telecom excitation wavelengths, we observed that this 'saturable photoexcited carrier refraction' yields a strong, negative nonlinearity from a phenomenological point of view [13], but we did not yet present a mathematical description for the refraction efficiency as a function of graphenes fundamental material properties [13]. Recently graphene's nonperturbative response was expressed as a function of its basic material characteristics using a semiconductor-physics-based formalism [15]. However, this fundamental approach is not necessarily the most practical way for describ-

ing time- and propagation-length-dependent optical excitations in waveguides, where the nonlinear response for a given electric field is typically described by means of a closed-form expression.

In this letter, we show that graphene's nonlinear refraction efficiency for time- and space-dependent excitations outside the perturbative regime can be predicted using an easily accessible formalism based on the so-called population recipe [14, 16]. More specifically, the refraction efficiency can be obtained from the excitation-induced instantaneous change in both temperature and chemical potential, and from the resulting instantaneous change in the *linear* conductivity of graphene, in line with the population recipe. We derive an expression that links the conductivity change with the commonly used  $n_{2,\text{gr}}$  and with the free-carrier refraction (FCR) coefficient  $\sigma_{\text{FCR}}$  introduced in [13]. Finally, we showcase the validity of our population-recipe-based formalism for a wide variety of four-wave mixing, self-(de)focusing and self-phase modulation experiments reported over the past decade.

## II. RATE EQUATION AND POPULATION RECIPE

Semiconductor nonlinearities resulting from the optical excitation of free carriers can often be described by means of the so-called population recipe, where the equilibrium carrier concentrations that enter into the *linear* conductivity are replaced by the photoexcited carrier concentrations [14, 16]. In this section we investigate whether this general ansatz for semiconductors could also hold for graphene. Let us assume a single-mode electric field propagating in the  $z$ -direction,  $\mathbf{E}(x, y, z, t) = A(z, t)/(\sqrt{4N}) \mathbf{e}(x, y, \omega_0) e^{-i\omega_0 t} e^{i\beta(\omega_0)z} + \text{c.c.}$ , where  $\omega_0$  is the mean spectral frequency of the light beam,  $N$  is a normalization constant such that  $|A(z, t)|^2$  equals the power,  $\mathbf{e}$  denotes the transverse distribution of the electric field, and  $\beta$  corresponds to the propagation constant. If a current density  $\mathbf{J}$  is produced due to the interaction between the electric field and a material such as graphene, exhibiting 1PA characterized by its conductivity  $\sigma_{ij}(\omega_0)$ , then the electromagnetic energy converted into free carriers per unit volume and unit time is given by  $\partial_t w = \mathbf{J} \cdot \mathbf{E} \approx |A(z, t)|^2 e_i^* \sigma_{ij} e_j / (2N)$ , where the last equation assumes a cycle averaging of the field [17]. In view of this equation, the dependence on space and time coordinates in  $w$  can be separated as  $w(x, y, z, t) = u(z, t)v(x, y)$ . Since  $u$  can show complex dependences on  $A$  as several carrier-related processes may exist, effective models are often employed to deal with these phenomena [13, 16]. Along the same

lines, we will study the temporal dynamics of the photoexcited carrier concentration based on the following rate equation for  $u$ :

$$\partial_t u = \left(1 - \frac{u}{u_{\text{sat}}}\right) |A(z, t)|^2 - \frac{u}{\tau_c}, \quad (1)$$

where  $u_{\text{sat}}$  and  $\tau_c$  are phenomenological parameters that account for saturation and decay mechanisms, respectively. The 1PA-induced carrier concentrations evolving in  $z$  and  $t$  can then be computed by means of a spatial average (over  $(x, y)$ ) of  $w/(\hbar\omega_0)$ . Although a more general modeling of carrier dynamics is possible [15], we showed in [13] that a rate equation like Eq. (1) can suffice to explain graphene's carrier-induced nonlinear effects.

Let us now explore how  $u$  behaves far from an equilibrium state where  $u$  is constant over time. Equation (1) can be solved by the integrating factor method,

$$\begin{aligned} \frac{u(z, t)}{u_{\text{sat}}} &= \int_{-\infty}^{\tau} \exp \left[ - \int_{\tau'}^{\tau} \left( \frac{T_0}{\tau_{\text{sat}}} U(z, \tau'') + \frac{T_0}{\tau_c} \right) d\tau'' \right] \\ &\times \frac{T_0}{\tau_{\text{sat}}} U(z, \tau') d\tau' \approx \frac{|A(z, t)|^2 / P_{\text{sat}}}{1 + |A(z, t)|^2 / P_{\text{sat}}}, \end{aligned} \quad (2)$$

where  $|A(z, t)|^2 = P_0 U(z, \tau = t/T_0)$ , with  $P_0$  and  $T_0$  being the input peak power and pulse width, respectively. To facilitate physical interpretation, a saturation time  $\tau_{\text{sat}} = u_{\text{sat}}/P_0$  and a saturation power  $P_{\text{sat}} = u_{\text{sat}}/\tau_c$  have been defined. The last step in Eq. (2) assumes  $T_0 \gg \tau_{\text{sat}}$  and  $T_0 \sim \tau_c$  (see e.g. [13]).

Important here is that Eq. (2) can be recovered from the steady-state solution of Eq. (1) ( $\partial_t u = 0$ ) if the time-independent steady-state power  $|A(z)|^2$  is replaced by the instantaneous power  $|A(z, t)|^2$ . Hence the photoexcited carrier densities in graphene could behave as carrier densities in 'instantaneous' steady states. As such, graphene's non-perturbative response could still be well described by means of the steady-state linear conductivity but with the carrier density at equilibrium replaced by the photoexcited densities calculated along Eq. (1). This carrier-induced instantaneous change in the linear conductivity then translates into the nonlinear response of the material.

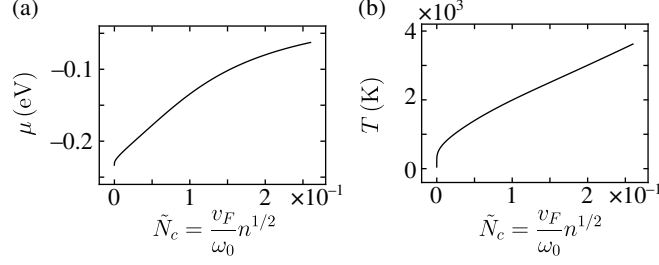


FIG. 1: Solutions of (a) Eq. (3) and (b) Eq. (4) plotted as a function of the normalized square-root of the carrier density, and with  $p_0 = 4 \times 10^{12} \text{ cm}^{-2}$  and  $\lambda_0 = 1.55 \mu\text{m}$ . The carrier densities range up to  $n_{\text{sat}} = 10^{17} \text{ m}^{-2}$  [13].

### III. NONLINEAR INDEX AND FREE-CARRIER REFRACTION COEFFICIENT

To implement the approach outlined above for modeling graphene's nonlinear response for propagating pulses in the non-perturbative regime, we need to determine explicit functional dependences of the chemical potential  $\mu$  and temperature  $T$  on the carrier concentration. To determine these, we consider that the probability of occupation of a state with energy  $E$  within the time scale of the excitation pulse is given by instantaneous Fermi-Dirac distributions. The density of states in graphene near the Dirac point is approximately  $\rho_{\text{gr}} = 2|E|/(\pi(\hbar v_F)^2)$ , where  $v_F \approx 10^6 \text{ m s}^{-1}$  is the Fermi velocity. The 2D densities of electrons  $n$  and holes  $p$  are calculated as  $n(\mu, T) = 2/(\pi(\hbar v_F)^2) \mu^2 J_1(\zeta)/\zeta^2$  and  $p(\mu, T) = 2/(\pi(\hbar v_F)^2) \mu^2 J_1(-\zeta)/\zeta^2$ , where  $\zeta = \mu/k_B T$ ,  $J_1(\zeta)$  is a Fermi-Dirac integral and  $k_B$  is the Boltzmann constant [18]. We aim at deriving closed expressions for  $\mu = \mu(n)$  and  $T = T(n)$  taking into account the electroneutrality condition, which relates  $n$  and  $p$ . To illustrate our approach we assume an initial hole density  $p_0$  [7, 8, 13], so  $p = p_0 + n$ .

To obtain explicit solutions  $\mu = \mu(n)$  and  $T = T(n)$ , we make use of two fitting functions and finally obtain:

$$\mu = -\left(\frac{\pi}{2\kappa_\mu}\right)^{1/2} \hbar v_F \frac{|\log(\eta)|}{\left(1 + \frac{1}{2\kappa_\mu} \log^2(\eta)\right)^{1/2}} (n + p_0)^{1/2} \quad (3)$$

$$k_B T = \left(\frac{\pi}{2\kappa_T}\right)^{1/2} \hbar v_F \frac{(n + p_0)^{1/2}}{\left(1 + \frac{1}{2\kappa_\mu} \log^2(\eta)\right)^{1/2}} \quad (4)$$

with  $\eta = n/(n + p_0)$ ,  $\kappa_\mu = 2.682$  and  $\kappa_T = 0.957$ . Note that for  $n = 0$ ,  $T = 0$  and

$\mu = -\hbar v_F(\pi p_0)^{1/2}$  are retrieved. For illustration the solutions of Eq. (3) and Eq. (4) for a commonly used  $p_0$  value of  $4 \times 10^{12} \text{ cm}^{-2}$  (see Section 4) are plotted in Fig. 1.

Now we turn to the imaginary part of graphene's conductivity at finite temperature, which can be calculated as [2]

$$\text{Im}[\sigma_{yy}^{(1)}(\omega, \mu, T)] = \frac{1}{2k_B T} \int_{-\infty}^{+\infty} \frac{\text{Im}[\sigma_{yy}^{(1)}(\omega, \tilde{x}, 0)]}{1 + \cosh\left(\frac{\tilde{x} - \mu}{k_B T}\right)} d\tilde{x}, \quad (5)$$

with the imaginary part of the conductivity at zero temperature given by

$$\text{Im}[\sigma_{yy}^{(1)}(\omega, \mu, 0)] = \frac{\sigma_0}{\pi} \left[ \frac{4|\mu|\hbar\omega}{(\hbar\omega)^2 + \Gamma_{\text{intra}}^2} - \frac{1}{2} \log \left( \frac{(2|\mu| + \hbar\omega)^2 + \Gamma_{\text{inter}}^2}{(2|\mu| - \hbar\omega)^2 + \Gamma_{\text{inter}}^2} \right) \right]. \quad (6)$$

Here  $\sigma_0 = e^2/4\hbar$  is the universal conductivity, and  $\Gamma_{\text{intra}}$  and  $\Gamma_{\text{inter}}$  are phenomenological scattering parameters for intraband and interband transitions, respectively. This result accounts for the interband and intraband motion of electrons around the Dirac cone at the single-particle level [1, 2]. Equation (5) with  $\mu$  and  $T$  as defined in Eq. (3) and Eq. (4), incorporating the effect of photoexcited carriers  $n[A(z, t)]$ , accounts for the carrier-induced instantaneous change in the imaginary part of the conductivity  $\text{Im}[\Delta\sigma_{yy}] = \text{Im}[\sigma_{yy}^{(1)}(n[A(z, t)]) - \sigma_{yy}^{(1)}(0)]$ , and provides graphene's time- and space-dependent nonlinear refractive response in the non-perturbative regime. As this is a closed-form expression, it is fully compatible with the nonlinear pulse propagation formalism commonly used for waveguides.

It should be noted that the quantity often measured in nonlinear experiments is the temporal average of the refractive index change  $\int_{-\infty}^{+\infty} \Delta n_{\text{gr}}(t) I(t) dt / \int_{-\infty}^{+\infty} I(t) dt$  where  $I(t)$  represents the instantaneous light intensity, and subsequently, the nonlinear index defined via  $n_2 = \int_{-\infty}^{+\infty} \Delta n_{\text{gr}}(t) I(t) dt / \int_{-\infty}^{+\infty} I^2(t) dt$ . Modeling graphene as a thin layer of 3D material as done in many experiments [3–5, 7–10], we derive the following expression to determine the magnitude and sign of the nonlinear index:

$$n_{2,\text{gr}} \sim -\frac{\pi \alpha^2 \lambda_0}{4} \frac{\text{Im}(\Delta\sigma_{yy}(n_{\text{sat}}/2)/\sigma_0)}{d_{\text{gr}} n_{\text{sat}}/2} \frac{\min(\tau_c, T_{\text{FWHM}})}{\hbar\omega_0}, \quad (7)$$

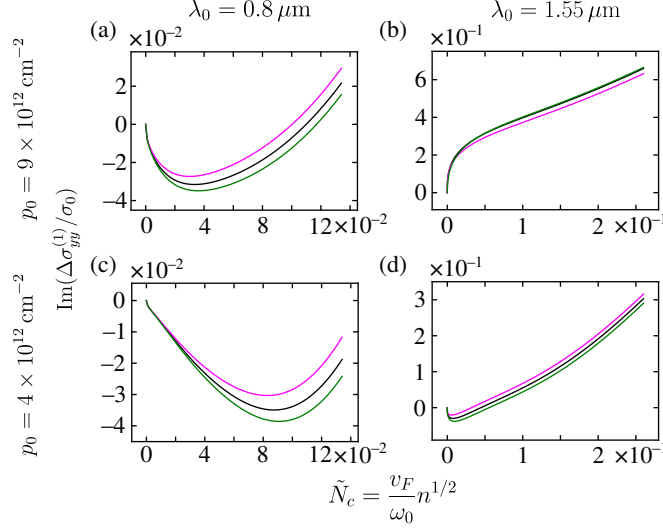


FIG. 2: (a)-(d) Imaginary part of the calculated dynamic conductivity change of graphene as a function of the normalized square-root of the carrier density, at two commonly used wavelengths and initial doping levels. The carrier densities range up to  $n_{\text{sat}} = 10^{17} \text{ m}^{-2}$  [13]. For illustration different scattering parameters are used [2]:  $\{\Gamma_{\text{inter}}, \Gamma_{\text{intra}}\} = \{33, 33\} \text{ meV}$  (black),  $\{65, 0.5\} \text{ meV}$  (magenta),  $\{0.5, 65\} \text{ meV}$  (green).

where  $\alpha = e^2/(4\pi\epsilon_0\hbar c) \approx 1/137$  denotes the fine-structure constant,  $d_{\text{gr}} = 0.33 \text{ nm}$  is the effective thickness of a single graphene sheet,  $n_{\text{sat}}$  is the saturation value of  $n$ , and  $T_{\text{FWHM}}$  indicates the full-width-at-half-maximum of the pulse duration.

In contrast to the works reporting a nonlinear index for graphene, we already analyzed our experiments with graphene-covered waveguides in [13] in terms of a nonlinear carrier-refraction response of the form  $-\sigma_{\text{FCR}}N_c$  embedded in the commonly used nonlinear pulse propagation formalism. Here  $N_c$  is a 1D carrier density defined at each  $z$ -distance along the waveguide. Since our approach in [13] resembles the modeling of silicon nonlinear-optical waveguides, we use [19] as our starting point to derive an expression for our FCR coefficient:

$$\sigma_{\text{FCR}} = \alpha \frac{v_F}{c} \frac{\text{Im}(\Delta\sigma_{yy}(\tilde{N}_{\text{sat}}/2)/\sigma_0)}{\tilde{N}_{\text{sat}}/2} \frac{\lambda_0}{4 n_{\text{eff}}} \frac{\int_{w_{\text{graph}}} |e_y(x_{\text{graph}}, y)|^2 dy}{\int_S |e_y(\mathbf{x}_t)|^2 dS}, \quad (8)$$

where  $e_y$  represents the  $y$ -component, parallel to the graphene sheet of width  $w_{\text{graph}}$ , of the waveguide's quasi-transverse electric-field mode,  $\tilde{N}_{\text{sat}} = (v_F/\omega_0)n_{\text{sat}}^{1/2}$ , and  $n_{\text{eff}}$  denotes the waveguide effective index. We point out that  $\sigma_{\text{FCR}}$  does not depend on  $d_{\text{gr}}$  nor on the pulse duration, making it a robust measure for graphene's nonlinear response.

#### IV. COMPARISON WITH EXPERIMENTS IN LITERATURE

Most of the experiments to measure graphene's nonlinearity at optical wavelengths have been performed using exfoliated or CVD graphene without intentional doping. As such, for most of those graphene samples the exact  $p_0$  value has not been measured. Taking into account the typical ranges of unintentional doping values, we assume estimated doping levels  $p_0 = 9 \times 10^{12} \text{ cm}^{-2}$  for exfoliated graphene [20] and  $p_0 = 4 \times 10^{12} \text{ cm}^{-2}$  for CVD graphene [21]. To illustrate the behavior of  $n_{2,\text{gr}}$  at two commonly used wavelengths, Figs. 2(a-d) show the calculated  $\text{Im}(\Delta\sigma_{yy}/\sigma_0)$  vs.  $\tilde{N}_c = (v_F/\omega_0)n^{1/2}$  at wavelengths  $\lambda_0 = 0.8 \mu\text{m}$  and  $\lambda_0 = 1.55 \mu\text{m}$  and at the estimated doping values for exfoliated and CVD graphene. Note that these graphs are robust against changes in the scattering rates  $\Gamma_{\text{intra,inter}}$ . According to these theoretical results and Eq. (7),  $n_{2,\text{gr}}$  is expected to switch sign between  $0.8 \mu\text{m}$  and  $1.55 \mu\text{m}$  with positive (negative) values at the shorter (longer) wavelengths. This prediction is in full agreement with the experiments reported so far, as can be seen in Table I. It also implies that graphene could be exploited as a material with a tunable nonlinearity sign in the near-infrared. Furthermore, our theory determines for the first time the (negative) sign for the graphene nonlinearity in Hendry's seminal experiment [3].

Besides predicting correct nonlinearity signs, Eq. (7) also provides orders of magnitude compatible with most  $n_{2,\text{gr}}^{\text{exp}}$  values in Table I (including the highest values), within its one-order-of-magnitude precision. This correspondence is a remarkable result as our calculations were carried out with *estimated* parameter values ( $p_0$  as specified above,  $n_{\text{sat}} = 10^{17} \text{ m}^{-2}$  and  $\tau_c = 1 \text{ ps}$  [13]). Eq. (7) also recovers the scaling of  $n_{2,\text{gr}}$  with pulse duration in the sub-ps excitation regime as experimentally observed in [8, 9].

Only for some of the experiments with very short (fs) pulses at short wavelengths, our theory appears to underestimate  $n_{2,\text{gr}}^{\text{exp}}$  by at least two orders of magnitude (see results marked with an asterisk in Table I). In those experiments the intraband carrier thermalization that follows right after the interband excitation might still be ongoing at the end of the pulse duration. As such, the intraband contribution to the conductivity change might not be important then, in which case a much higher positive nonlinearity value could be produced by theory. Further theoretical developments will be required to check this hypothesis. This being said, the easily accessible theory presented here does yield a good match with all other data in Table I observed for different pulse lengths (ps and sub-ps). This underlines

Work	$\lambda$ (nm)	$p_0^{\text{estimated}}$ ( $\text{cm}^{-2}$ )	$T_{\text{FWHM}}$ (ps)	$I_0$ ( $\text{W m}^{-2}$ )	$n_{2,\text{gr}}^{\text{exp}}$ ( $\text{m}^2 \text{W}^{-1}$ )	$\text{Im}(\Delta\sigma_{yy}(n_{\text{sat}}/2)/\sigma_0)$	$n_{2,\text{gr}}^{\text{theo}}$ ( $\text{m}^2 \text{W}^{-1}$ )
[4]	733	$4 \times 10^{12}$	0.1	$9 \times 10^{14}$	$1 \times 10^{-13}$	$-3.6 \times 10^{-2}$	$2 \times 10^{-14}$
[9]	900	$4 \times 10^{12}$	0.1	$5 \times 10^{13}$	$1 \times 10^{-12}$	$-1.0 \times 10^{-2}$	$1 \times 10^{-14*}$
[9]	900	$4 \times 10^{12}$	0.475	$5 \times 10^{13}$	$2 \times 10^{-12}$	$-1.0 \times 10^{-2}$	$5 \times 10^{-14}$
[8]	1550	$4 \times 10^{12}$	3.8	$5 \times 10^{12}$	$-2 \times 10^{-12}$	0.18	$-6 \times 10^{-12}$
[7]	1553	$4 \times 10^{12}$	3	$2 \times 10^{13}$	$-4 \times 10^{-13}$	0.17	$-5 \times 10^{-12}$
[8]	1600	$4 \times 10^{12}$	0.18	$5 \times 10^{12}$	$-1 \times 10^{-13}$	0.19	$-1 \times 10^{-12}$
[6]	2400	$4 \times 10^{12}$	0.1	$2 \times 10^{14}$	$-3 \times 10^{-13}$	0.74	$-5 \times 10^{-12}$
[10]	355	$9 \times 10^{12}$	10	$1 \times 10^{14}$	$5 \times 10^{-16}$	$-1.4 \times 10^{-2}$	$2 \times 10^{-14}$
[5]	800	$9 \times 10^{12}$	0.015	$3 \times 10^{15}$	$\pm 2 \times 10^{-11}$	$-1.0 \times 10^{-2}$	$1 \times 10^{-15*}$
[3]	1000	$9 \times 10^{12}$	6	$1 \times 10^{13}$	$\pm 4 \times 10^{-13}$	$6.1 \times 10^{-2}$	$-8 \times 10^{-13}$

Work	$\lambda$ (nm)	$p_0^{\text{measured}}$ ( $\text{cm}^{-2}$ )	$T_{\text{FWHM}}$ (ps)	$I_0$ ( $\text{W m}^{-2}$ )	$\sigma_{\text{FCR}}^{\text{exp}}$	$\text{Im}(\Delta\sigma_{yy}(\tilde{N}_{\text{sat}}/2)/\sigma_0)$	$\sigma_{\text{FCR}}^{\text{theo}}$
[13]	1563	$6.5 \times 10^{12}$	3	$3 \times 10^{12}$	$(1 \pm 0.2) \times 10^{-5}$	0.26	$0.7 \times 10^{-5}$

TABLE I: Comparative table of the magnitudes and signs of graphene’s experimental  $n_{2,\text{gr}}$  and  $\sigma_{\text{FCR}}$  values and the theoretical values calculated by means of Eq. (7) and Eq. (8) with estimated parameter values  $n_{\text{sat}} = 10^{17} \text{ m}^{-2}$  and  $\tau_c = 1 \text{ ps}$  [13]. The symbol  $\pm$  indicates that the sign of  $n_{2,\text{gr}}^{\text{exp}}$  could not be determined in those experiments. \* See text for a detailed discussion of these cases.

the general applicability of our population-recipe-based model for a wide range of excitation conditions.

Finally, we want to emphasize that  $\sigma_{\text{FCR}}$  as specified in Eq. (8) is a more robust parameter than  $n_{2,\text{gr}}$  to quantify graphene’s nonlinear response outside the perturbative regime. For the  $\sigma_{\text{FCR}}$  value that we extracted from our experiments with graphene-covered waveguides [13], we find an excellent agreement with our theoretical prediction (see bottom of Table I).

In conclusion, with our population-recipe-based theory we can adequately predict graphene’s nonlinear refractive response for propagating pulses outside the perturbative regime. With the obtained expressions for  $n_{2,\text{gr}}$  and  $\sigma_{\text{FCR}}$ , one can readily calculate how the response evolves over time and distance. Our work clarifies the differences in sign and magnitude of graphene’s nonlinear coefficients measured over the past decade, and provides an essential tool for predicting the performance of nonlinear-optical graphene-enhanced waveguide devices.

## FUNDING INFORMATION

This work was supported by the ERC-FP7/2007-2013 grant 336940 and the Research Foundation Flanders (FWO) under Grants GA00213N, G0F6218N (EOS-convention 30467715),

VUB-OZR and FWO postdoctoral fellowship (147788/12ZN720N).

---

- [1] J. L. Cheng *et al.*, *New J. Phys.* **16**, 053014 (2014).
- [2] J. L. Cheng *et al.*, *Phys. Rev. B* **91**, 235320 (2015).
- [3] E. Hendry *et al.*, *Phys. Rev. Lett.* **105**, 097401 (2010).
- [4] W. Chen *et al.*, *AIP Advances* **3**, 042123 (2013).
- [5] R. Ciesielski *et al.*, *Nano Lett.* **15**, 4968 (2015).
- [6] G. Demetriou *et al.*, *Opt. Express* **24**, 13033 (2016).
- [7] N. Vermeulen *et al.*, *Phys. Rev. Appl.* **6**, 044006 (2016).
- [8] E. Dremetsika *et al.*, *Opt. Lett.* **41**, 3281 (2016).
- [9] S. Thakur *et al.*, *Sci. Rep.* **9**, 10540 (2019).
- [10] H. Wang *et al.*, *Opt. Mater. Express* **9**, 339 (2019).
- [11] T. Jiang *et al.*, *Nat. Photonics* **12**, 430 (2018).
- [12] K. Alexander *et al.*, *ACS Photonics* **5**, 12, 4944 (2018).
- [13] N. Vermeulen *et al.*, *Nat. Commun.* **9**, 2675 (2018).
- [14] P. Butcher and D. Cotter, Cambridge Univers. Press (1990).
- [15] M. Baudisch *et al.*, *Nat. Commun.* **9**, 1018 (2018).
- [16] D. N. Christodoulides *et al.*, *Adv. Opt. Photon.* **2**, 60 (2010).
- [17] J. D. Jackson, John Wiley & Son, Inc. (1975).
- [18] T. Fang *et al.*, *Appl. Phys. Lett.* **91**, 092109 (2007).
- [19] Q. Lin *et al.*, *Opt. Express* **15**, 16604 (2007).
- [20] J. M. Caridad *et al.*, *J. Appl. Phys.* **108**, 084321 (2010).
- [21] T. Ciuk *et al.*, *J. Phys. Chem. C* **117**, 20833 (2013).